SciTech2015
5-9 January, 2015, Kissimmee, FL
53rd AIAA Aerospace Sciences Meeting

Near Field Sonic Boom Calculation of Benchmark Cases

Jiaye Gan*, Gecheng Zha†
Dept. of Mechanical and Aerospace Engineering
University of Miami
Coral Gables, FL 33124
gzha@miami.edu

Abstract

This paper validates the accuracy of a high order accuracy CFD code on predicting near field signatures of sonic boom propagation. The flow near the body is solved using a structured grid Euler solver with low diffusion E-CUSP schemes, 3rd order MUSCL scheme, and 3rd and 5th order WENO schemes. Three benchmark cases, including two non-lifting models and one lifting model, are calculated. The predicted results are in good agreement with that of experiment data. For the Delta wing configuration, the mesh provided by the workshop generates a smooth expansion wave at the off-track plane. When the mesh is refined, a shock coalesced by the compression waves from the wing tip is captured and it generates a weak shock wave interacting with the expansion.

1 Introduction

Although the Concorde, the first supersonic civil transport ceased service in 2003 due to high operating costs, efforts to minimize the sonic boom and make supersonic commercial flight economically and environmentally viable continues. To design a supersonic airplane with low sonic boom, an accurate simulation tool is essential. However, resolving accurate shock propagation is very challenging due to numerical dissipation. The current sonic boom prediction methodology is to simulate the near field with fine mesh resolution. From near field to ground, the shock wave propagation and compression wave coalesce are simulated by linear wave equations [1] or nonlinear Burger's equations [2].

Many efforts have been made in the past 2 decades to develop an accurate sonic boom prediction methodology. Rallabhandi et al[3] develop a mixed-fidelity CFD-based low-boom design process to design and evaluate low-boom configurations. The NASA FUN3D CFD code is used to calculate the gradient from ground boom signature instead of the near field signature. Elmiligui et al[4] employ two NASA codes, USM3D (Navier-Stokes) and CART3D-AERO (Euler, adjoint-based adaptive mesh), to compute off-body sonic boom pressure signatures at several altitudes at Mach 2.0. The computed pressure signatures agrees well with wind tunnel data. Wintzer et al [5] develop a multi-level framework for the design of low sonic boom aircraft. The NASA Cart3D CFD code with ajoint-driven mesh refinement is used to construct high quality volume grid. Ishikawa et al [6] develop a structured/unstructured overset grids method for predicting sonic-boom. The unstructured grid CFD is used around the airplane and the structured grid CFD solver is used to predict the near-field pressure signatures. The CFD

* Ph.D. Candidate
† Ph.D., Professor, Director of Aerodynamics and CFD Lab

code UPACS(Unified Platform for Aerospace Computation Simulation) is adopted as a high-fidelity aerodynamic analysis in their study in order to verify the S3TD design results.

A workshop was organized by NASA to evaluate new-field sonic boom prediction capability in Oct of 2008 [7]. The sonic boom signatures of three non-lifting bodies and two lifting configurations were computed. The results from AIRPLANE, Cart3D, FUN3D, and USM3D flow solvers were evaluated in the workshop. Reasonable results were produced and the accuracy of the available methods exceeded the expectations of the participants. The AIAA First Sonic Boom Prediction Workshop[8] held in Jan of 2014 assessed the state of the art of near field sonic boom prediction. Blind tests of various computational models were conducted without prior knowledge of the experiment data. Comparisons were made among participants' solutions on workshop provided grids. Numerical results are in good agreement with experiment data in general. Participants also reach a conclusion that Mach cone alignment and stretching along Mach rays are important for accurate sonic boom predictions for all types of grid methods.

This paper compares the accuracy of near filed sonic boom prediction using different shock capturing schemes for the benchmark cases provided by the AIAA 2014 Sonic Boom workshop[8]. The effects of turbulence modeling on sonic boom prediction are evaluated by the simulation of a NASA cone[9].

2 Numerical methods

The in house high order accuracy CFD code FASIP(Flow-Acoustic-Structure Interaction Package), which is intensively validated with various 2D and 3D steady and unsteady flows including sonic boom[10, 11, 12, 13, 14], is used in this paper. To accurately capture shock waves, high order shock capturing schemes, including 3rd order MUSCL scheme[15], 3rd, 5th and 7th order WENO schemes and a finite compact scheme combining a shock detector and 6th order Pade scheme, are implemented in the code[12, 13, 14, 16]. A set of 4th order and 6th order central differencing schemes are devised to match the same stencil width of the WENO schemes for the viscous terms[17, 18]. For turbulent simulations, FASIP has implemented Detached Eddy Simulation (DES)[19, 20, 21, 22, 23, 24, 25], Large Eddy Simulation(LES)[18, 26], and Reynolds averaged Navier-Stokes (RANS)[27, 17, 28, 29, 30, 31, 32, 33]. An implicit 2nd order time accurate scheme with pseudo time and unfactored Gauss-Seidel line relaxation is employed for time marching. For aeroelasticity problems, a fully coupled fluid-structural interaction model is implemented[34, 25, 33, 21, 27, 29, 30, 20]. The MPI parallel computing is utilized and a high scalability is achieved[35]. In this paper, the Roe's scheme[36] and a low diffusion E-CUSP scheme developed by Zha et al[37] are used as the approximate Riemann solver with the 3rd order MUSCL, 3rd and 5th order WENO schemes to evaluate the inviscid fluxes.

3 Results and discussion

Due to symmetry about the longitudinal axis, all the configurations are simulated with half of the geometry to save CPU time using symmetric boundary conditions on the central plane at zero span. The inviscid Euler solver is used for all the cases. For the NASA cone, RANS solver is used to compare the results with the Euler solver.

3.1 NASA cone

The cone Model 1 in the NASA sonic boom wind tunnel testing[9] is used to validate the CFD mesh setup and numerical schemes selection. The half cone angle is 3.24° and the cone length is 2 inch. The experimental Mach numbers 2.01 is calculated for its near field sonic boom signature. The computed

results are compared with the experiment[9] and the CFD results of Wintzer et al[38]. The far field sonic boom signature is extrapolated using the NASA *NF Boom* code [1] based on the method of Thomas[39].

The cone Model 1[9] is simulated with half geometry as shown in Fig. 1. The FASIP code is a point to point connected structured grid flow solver, so special treatment should be done to remove the singularity at the tip of the cone as shown in Fig. 1. The tip of cone is rounded with diameter less than 0.0001 of the cone maximum diameter. An small O-type mesh topology is applied to the tip of the cone as shown in Fig. 1, so that a fully point to point connected mesh topology can be generated. A cross section of the mesh is shown in Fig. 2. The mesh is inclined at the Mach angle to resolve the oblique shock waves. The computational domain size is extended one body length upstream, two and a half body length above and below the cone, and four and half body length downstream of the cone. The inlet boundary conditions is to fix all the variables at the freestresm conditions. The upper, lower, and downstream conditions are zero gradient extrapolation. As the initial trails, the RANS model with Baldwin-Lomax model was used and the near field sonic boom was significantly over-predicted due to the boundary layer thickness. The calculation is then switched to inviscid calculation as the methods used by other groups[40, 38, 41, 42]. The rear part of the cone with constant radius cylinder is extended to the exit boundary for the simplicity of boundary condition treatment. The baseline mesh for the inviscid Euler solver is $201 \times 141 \times 61$ in the streamwise, radial and circumferential direction respectively.

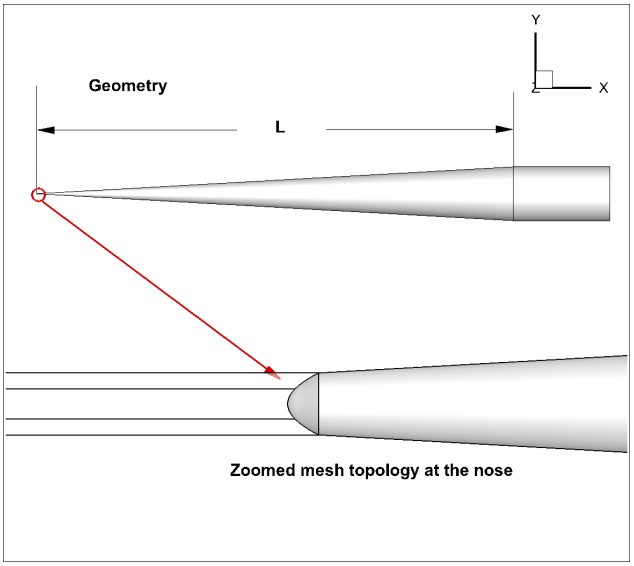

Figure 1: Geometry and mesh topology for NASA cone Model 1[9].

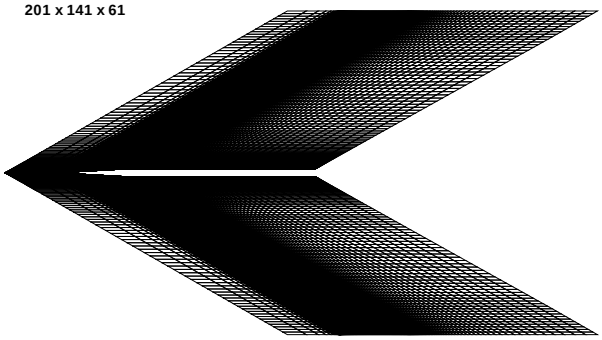

Figure 2: Cross section of the mesh for NASA cone Model 1.

Grid independent study is conducted with two different grid sizes for the Euler solver. The baseline mesh is used as the coarse mesh with a total number of 1.72 million grid points and the refined mesh is 7.42 million with grid dimension of $331 \times 222 \times 101$. The CFL number is 1.0 with the implicit time integration scheme. Fig. 3 is the near field pressure signature at $H/L = 2$, where H is the vertical distance from the cone leading edge and L is the cone length.

Fig. 3 shows that computed pressure signatures of both coarse mesh and refined mesh agree excellently with the computed results from [38], which has been validated with experiment. It indicates that the over pressure signature computed using the baseline mesh is converged. The comparisons of different numerical scheme results are shown in Fig. 4. It can be seen that all the schemes have the same results as that from [38]. Fig. 5 is the extrapolation to $H/L = 10$ using the NASA *NF Boom* code[1] and excellent agreement with the experimental measurement is achieved.

Fig. 6 is the computed over-pressure with different turbulence models. A refined mesh is used in

turbulence model test $Y^+ = 1$. It can be seen that results with turbulence model over predict the overpressure compared with that of inviscid model. Fig. 7, 8, 9 are the Mach contours of the cone Model 1 at incoming Mach number of 2.01. The viscous calculation has a boundary layer on the cone surface, which appears to be the cause for the over-pressure prediction discrepancy from the Euler solver. It indicates the sensitivity and challenges of shock prediction in viscous flows. More efforts are needed to make it more accurate.

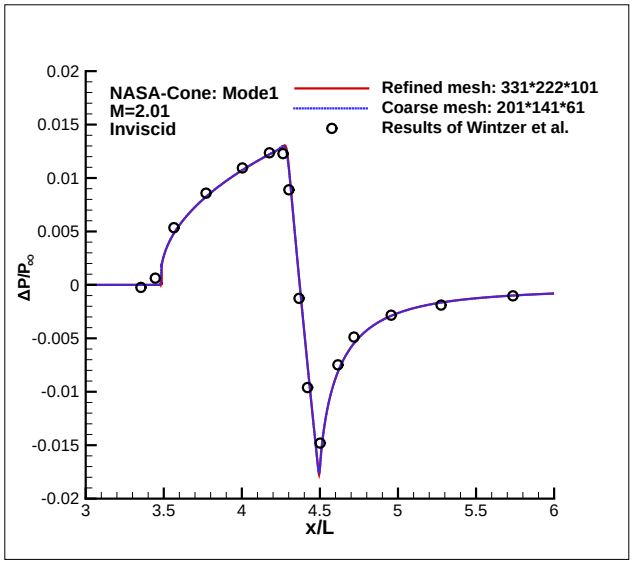

Figure 3: Comparison of the computed over-pressure at two and half body lengths below the cone Model 1 for mesh refinement study.

3.2 SEEB-ALR

The axisymmetric Seeb-ALR model was a required model in 1st AIAA sonic boom workshop. The model is a non-lifting body and featured of flat-top pressure signature, which was created based on the theory of Christine Darden's nose bluntness relaxation. The model was constructed by Lockheed Martin and was tested in the NASA Ames 9-7 ft. Supersonic Tunnel in 2012[8]. The SEEB design transits monotonically to cylindrical aft-bodies. The transition is intentionally designed with non-smooth 2nd order derivative. A reference length of L=17.667in is specified for the workshop and the body reaches its maximum diameter of 1.43in around 15.6in from the tip. The cylindrical sting has a diameter of 1.395in. which begins 17.678in. downstream of the tip. The sting is tapered to a point far downstream in the simulations. Only the inviscid Euler solver is used for this case.

Grid alignment with mach cone angle is shown in Fig. 10. As the NASA cone case, the mesh of SEEB-ALR also employs a tiny radius with O-type of mesh topology at the tip of nose to make the grids point to point connected, see Fig. 11. Two types of mesh were tested. The grid sizes of coarse mesh are 2.22 million with dimension of $65 \times 97 \times 353$ and the refined mesh has 7.42 million with dimension of $97 \times 129 \times 593$ in circumferential, radial and streamwise direction respectively. Fig. 12 and 13 show the computed results of over-pressure for the coarse mesh and refined mesh respectively. An excellent agreement among the computed results of all the different schemes is obtained. The geometry 2nd order derivative oscillation is very well captured as shown by the saw teeth oscillation at the flat top and at the expansion flat part. Fig. 14 is the comparison of signatures between the coarse mesh and refined mesh with Zha [37] flux splitting and 3rd order WENO scheme. They agree excellently overall except the refined mesh has slightly stronger saw teeth fluctuation for the flat top of the signature. Fig. 15

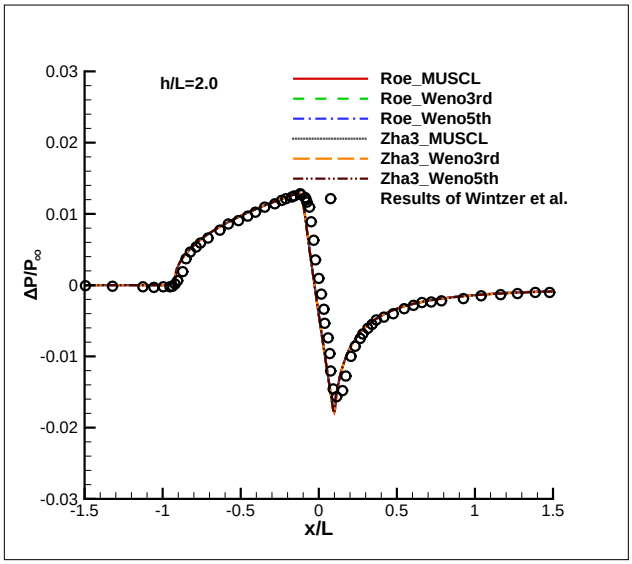

Figure 4: Computed Over-pressure at two body lengths below the cone Model 1 compared with the result from[38].

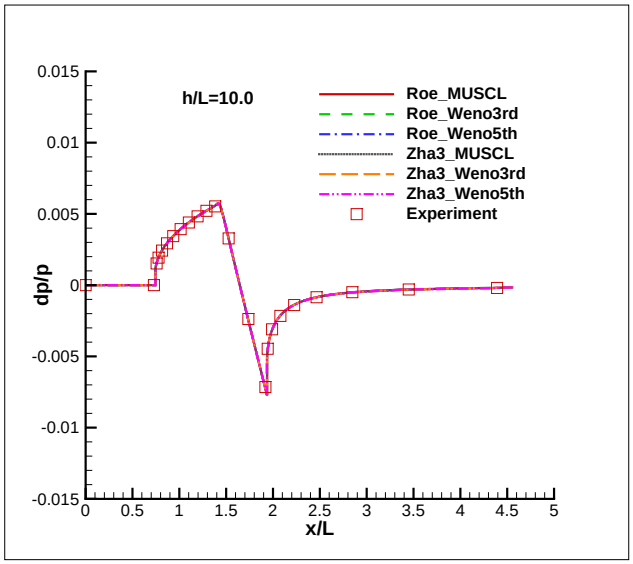

Figure 5: Computed Over-pressure at ten body lengths below the cone Model 1 compared with experiment[9].

and Fig. 16 are the contour plots of Mach number and pressure respectively. The saw teeth waves and their propagation are very well captured. It also indicates that the Euler solver of FASIP code is highly responsive to wave perturbation and propagation.

3.3 69° delta wing body

The second required model is the NASA 69° delta wing-body [43] configuration. The geometry of the delta wing body is shown in Fig. 17. The model is a 17.52 inches long. The delta wing body provided by the workshop is the 4th model in a series of sonic boom tests of models with different planforms. The wing thickness to chord ratio is 0.05 and the leading edge sweep is 69°. The Mach number is 1.68 and the angles of attack are varied from 0 to 4.74 degree to correspond to the available test data. This configuration was chosen because it is a simple lifting geometry. Again, only the inviscid Euler solver is used for this case to focus on predicting the shock wave and over pressure accurately.

There are 4 singular grid points in the original mesh provided by the workshop as shown in Fig. 18, which can not be used directly for FASIP. Hence, modifications on the mesh topology are necessary to make the grid to be point to point connected. First, the singularity at the tip of the nose is replaced by the tiny radius of O-type mesh topology as in the NASA cone and SEEB-ALR geometry, see Fig. 19. Second, the other three singular points can be avoided by splitting the leading edge side of the triangle wing into two connectors and form a quadrangle on the delta wing, see Fig. 20. The mesh size is 129×129 on the wing surface, but the number of the grid points along the swept wing leading edge is doubled compared with the original mesh of the work shop. The increased mesh points along the wing leading edge also increase the mesh points off the wing in the near field. The effect of mesh topology and mesh size on the wing will be discussed later. The mesh topology and physical domain of the delta wing body are shown in Fig. 21 and Fig. 22 respectively. There are total 12.21 millions grid points in the mesh, which are split into 174 blocks for parallel calculation.

Fig. 23 shows the predicted over-pressure compared with the experiment at AoA=4.74° and h/l=3.6. It can be seen that the bow and wing shocks are in good agreements with experiment[43]. Fig. 24 is the on-track(symmetry plane) and off-track(away from symmetry plane) signatures at h=31.8 inches for

AoA=0. The computed over-pressure has a good agreement with experiment data. However, there is a weak shock wave during the expansion from wing tip as shown in the results of off-track signal(phi=90° and 60°), which is not captured by the measurement and other participants of the workshop.

In order to investigate the cause of the weak shock in the expansion, two slightly modified meshes are created. The mesh we used with the split point at the center of the swept wing leading edge to avoid the singularity points makes the total number grids more than that of original workshop mesh. The workshop surface mesh is129×129 and our mesh without singularity points is also 129×129, but our new topology increases the number of mesh points off the wing surface in the near field. Hence the first modified mesh is to keep the same mesh density as the original mesh on wing surface. It is found that if the side connected with the cylinder body is split, the mesh sizes off the wing can be kept exactly the same as the workshop mesh, see Fig. 25. The predicted over-pressure of the mesh with the same workshop mesh off the wing is shown in Fig. 26. It can be seen that weak shock in the expansion off-track disappears. Therefore the weak shock in the expansion appears to be caused by refined mesh off the wing in the near field. To further verify this discovery, a refined mesh based on the work shop near field mesh with the same topology is made. The other refined mesh that employs the same topology as the first new mesh, but the mesh density becomes 161×161 on the wing surface. There are about 24.04 million cells in the refined mesh, which is split into 313 blocks for parallel computation. Fig. 27 shows the predicted over-pressure of the refined mesh at h=31.6 inches. It can be seen clearly that the weak shock wave is captured again in the expansion.

Fig. 28 shows the Mach contours and shock wave pattern of the coarse mesh at off-track plane. There are no shock wave in the expansion from the wing tip. Fig. 29 show the Mach number contours of the refined mesh at the same position as that of coarse mesh. The weak shock is clearly seen due to the coalesce of a series of compression waves. Fig. 30, 31, 32, 33 compare the Mach number contour and shock wave structure at different angle of attack at the on-track plane. It can be seen that the shock near the trailing edge become stronger as the the AoA increases. Fig. 34, 35, 36, 37 compared the surface isentropic mach number contours at different angle of attack. The shock starting from wing tip become stronger as the AoA increases.

4 Conclusions

This paper focus on validating the accuracy of an in house code on predicting near field signatures for sonic boom propagation. The flow near the body is solved using an Euler solver with low diffusion E-CUSP schemes. Three benchmark cases, two non-lifting models and one lifting model are calculated. Different flux splitting and reconstruction schemes that are frequently used in the code are tested. The predicted results have a good agreement with that of experiment data. A careful study to evaluate the mesh resolution for the accurate capture of the shock wave is conducted for the delta wing body configuration. The mesh provided by the workshop generates a smooth expansion wave at the off-track plane. When the mesh is refined, a shock coalesced by the compression waves from the wing tip is captured and it generates a weak shock wave interacting with the expansion.

5 Acknowledgment

The computing resource support from the Center for Computational Sciences at University of Miami is greatly appreciated.

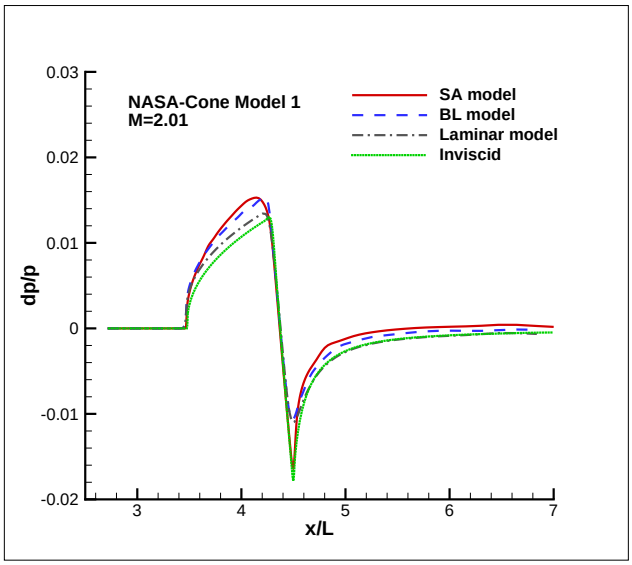

Figure 6: Computed Over-pressure with different turbulence model at two body lengths.

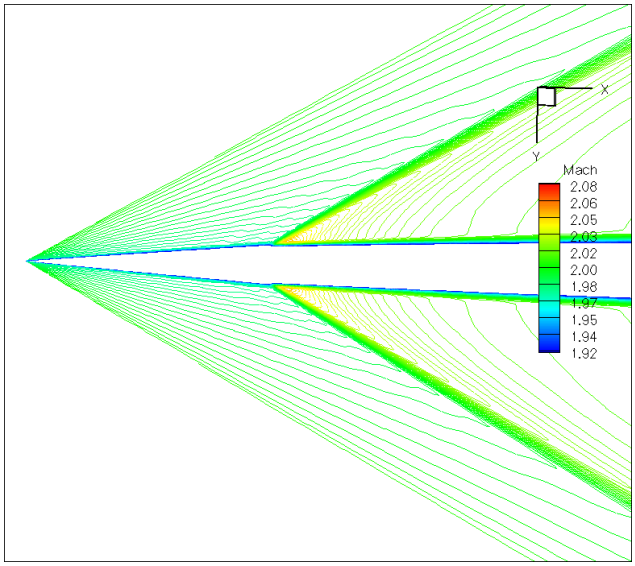

Figure 7: Mach contours with BL turbulent model

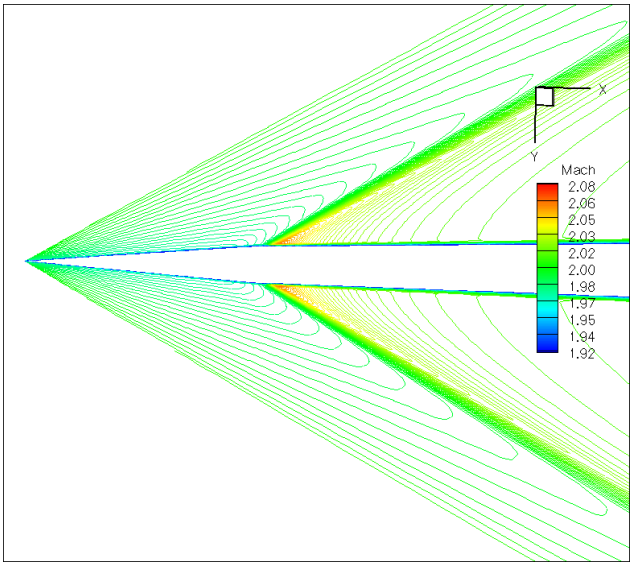

Figure 8: Mach contours with SA turbulent model.

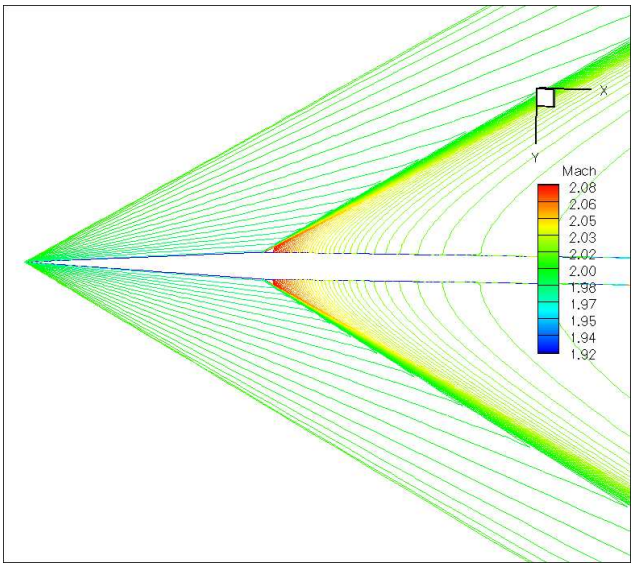

Figure 9: Mach contours with inviscid model.

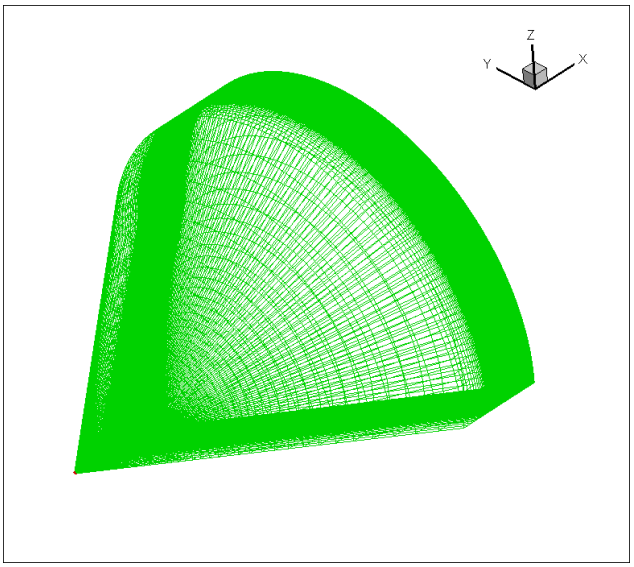

Figure 10: Mach cone alignment mesh

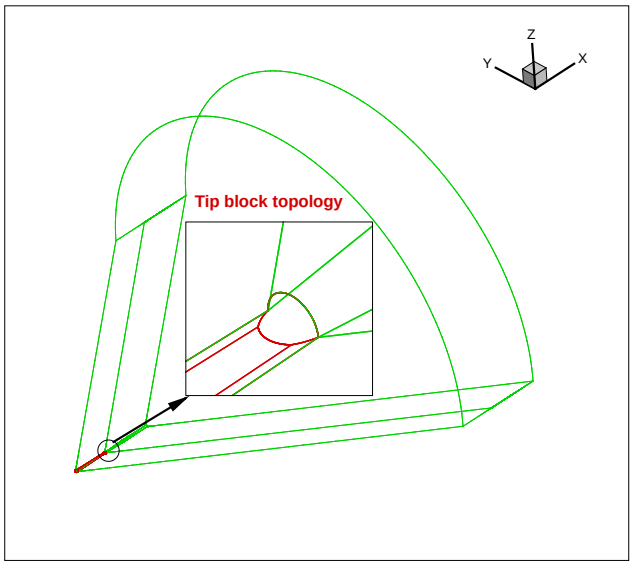

Figure 11: Grid topology of the numerical domain

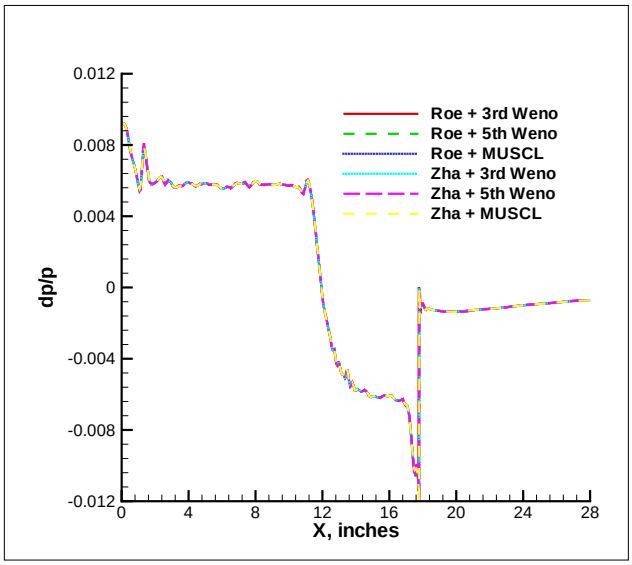

Figure 12: Extracted near field signatures with different schemes of the coarse mesh

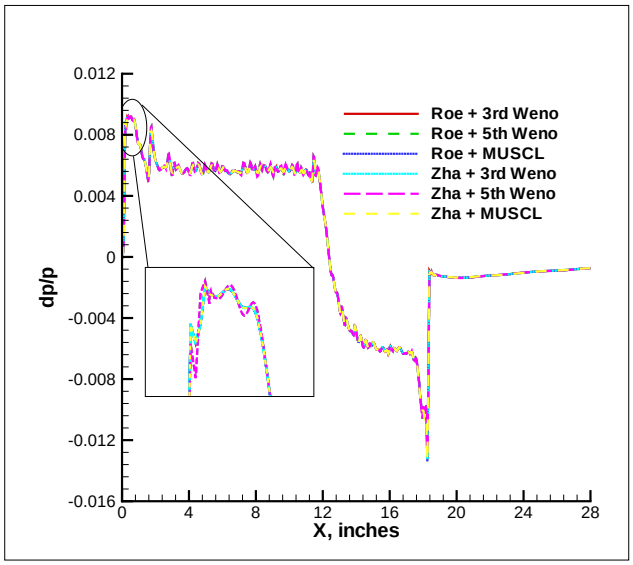

Figure 13: Extracted near field signatures with different schemes of the refined mesh

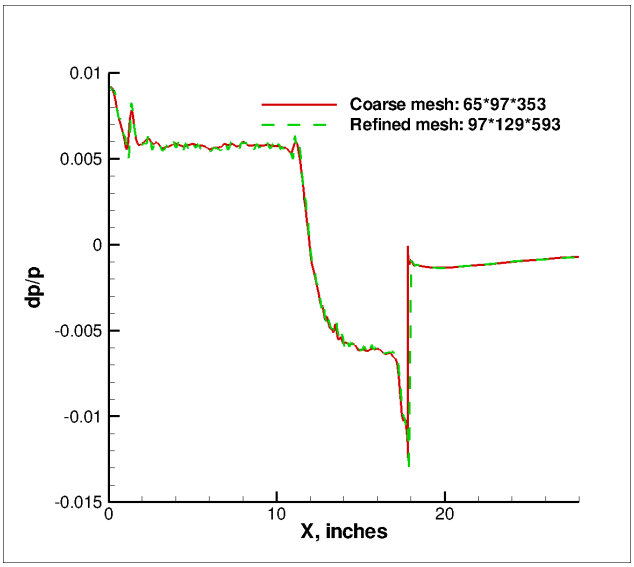

Figure 14: Mesh resolution comparisons with the 3rd-Weno schemes

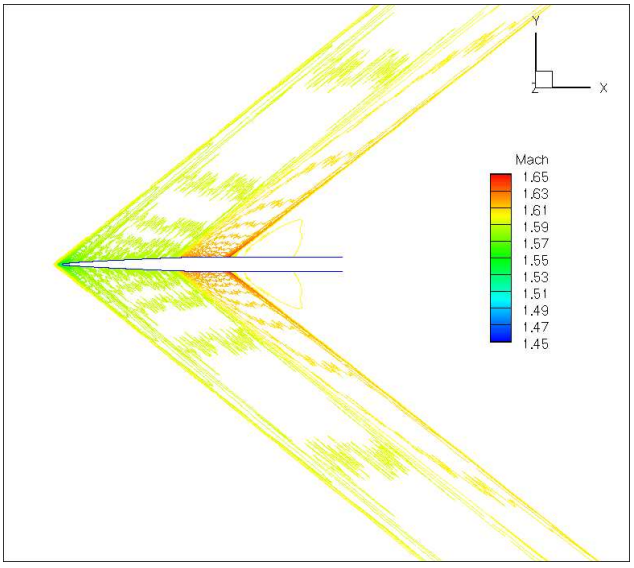

Figure 15: Mach line contour

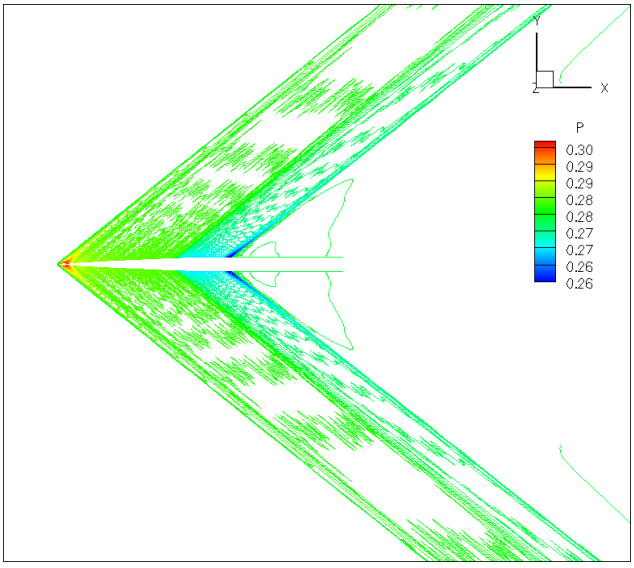

Figure 16: Pressure line contour

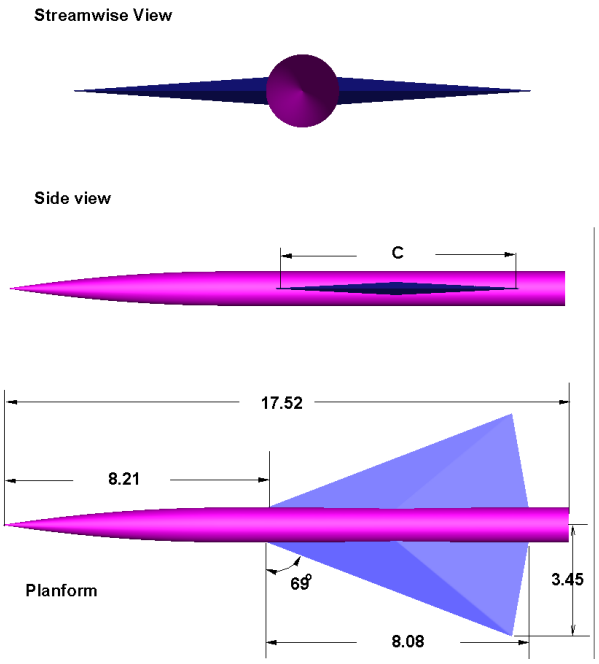

Figure 17: Geometry of delta wing

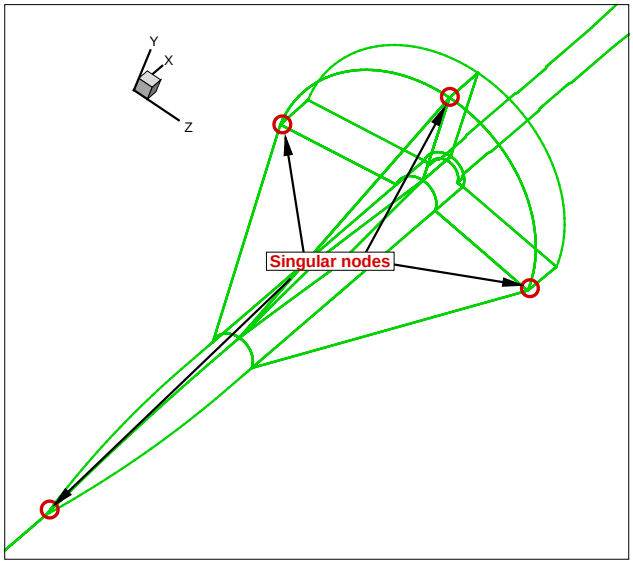

Figure 18: Original mesh topology from the sonic boom workshop

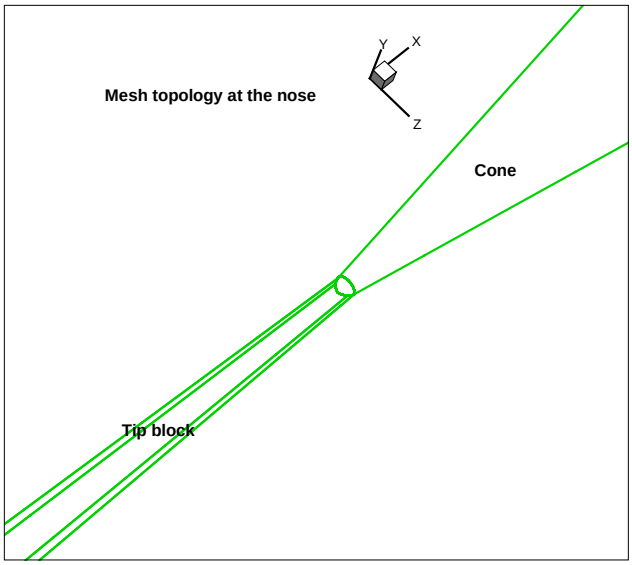

Figure 19: Tip mesh topology of Delta wing.

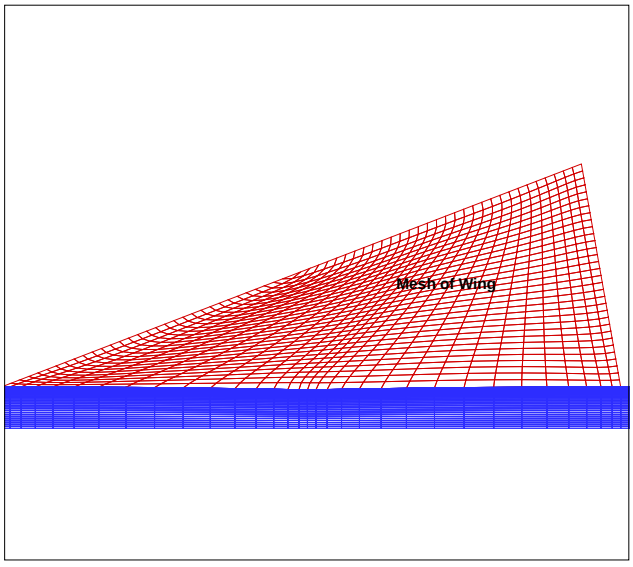

Figure 20: Mesh topology on the wing with 129×129 grids. For view purpose, it was coarsen in the plot

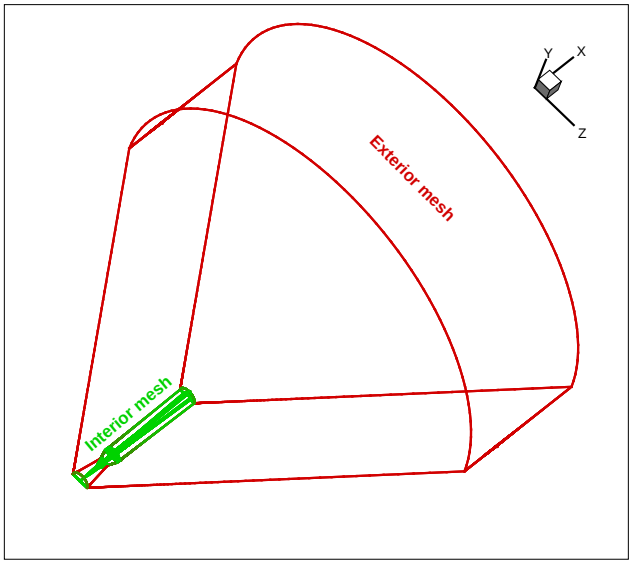

Figure 21: Mesh topology of the domain.

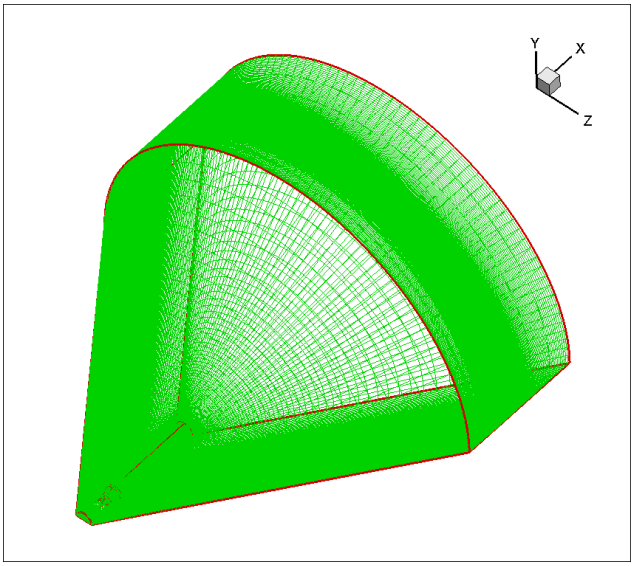

Figure 22: 3D mesh of delta wing.

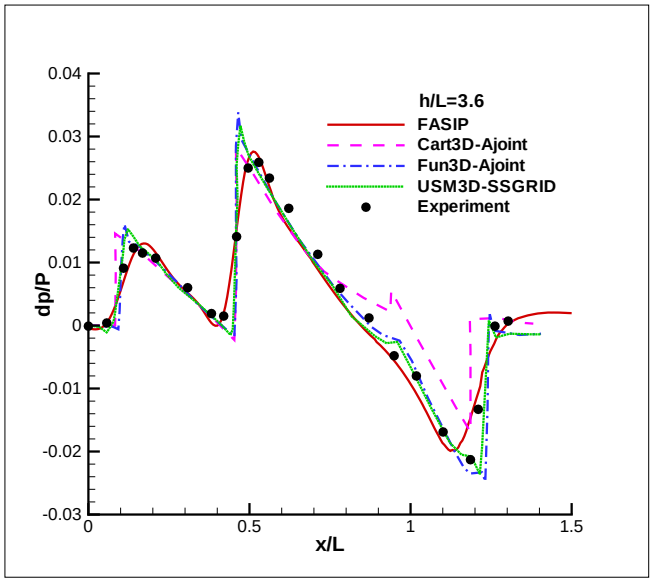

Figure 23: Extracted dp/p at AoA=4.74 and h/l=3.6

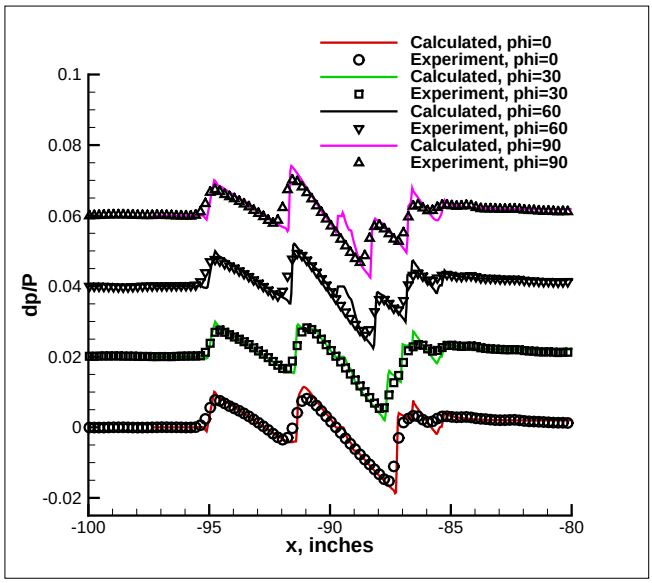

Figure 24: Extracted dp/p of mesh 1 at AoA=0.0 and h=31.6 inches

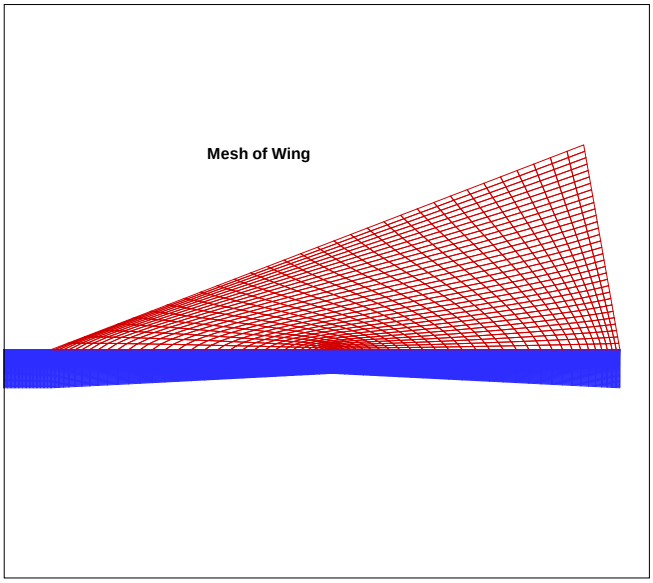

Figure 25: Mesh topology on the wing with 129*129 grids. For view purpose, it was coarsen in the plot

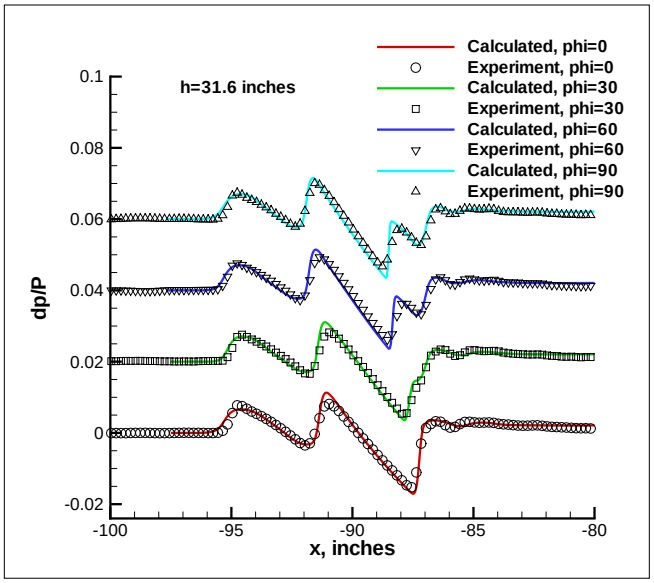

Figure 26: Extracted dp/p of mesh 2 at AoA=0.0 and h=31.6 inches

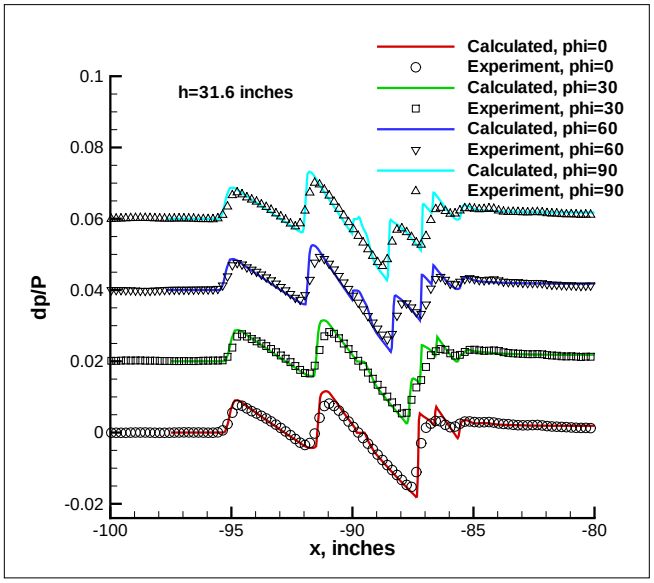

Figure 27: Extracted dp/p of mesh 3 at AoA=0.0 and h=31.6 inches

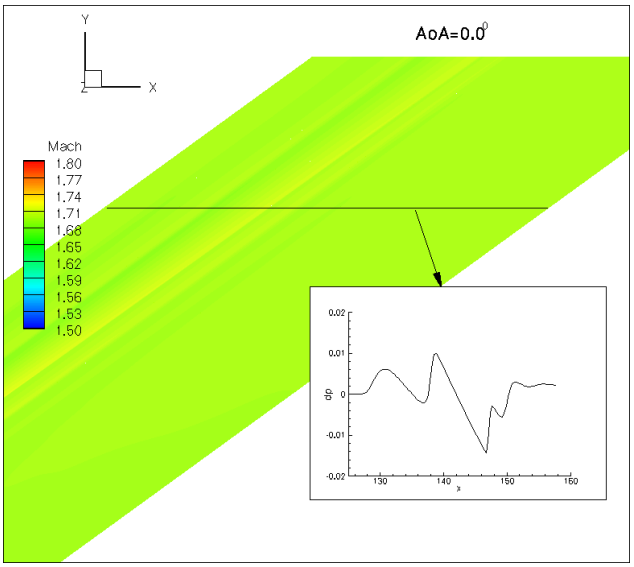

Figure 28: Shock wave pattern of coarse mesh in 90 degree plane

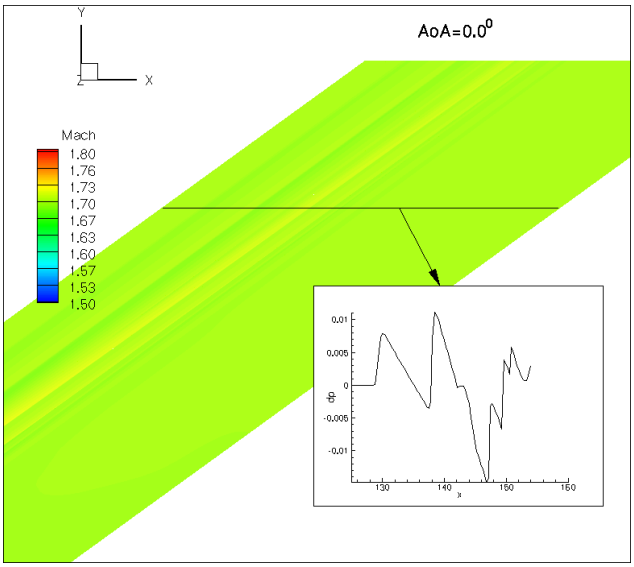

Figure 29: Shock wave pattern of refined mesh in 90 degree plane

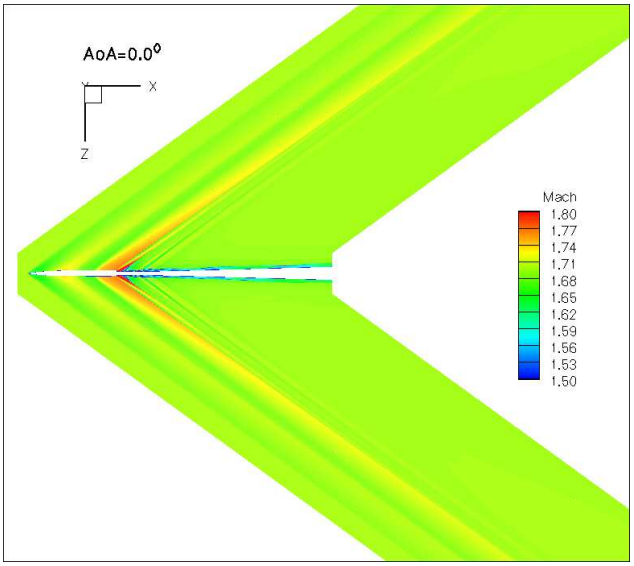

Figure 30: Mach contours at AoA=0

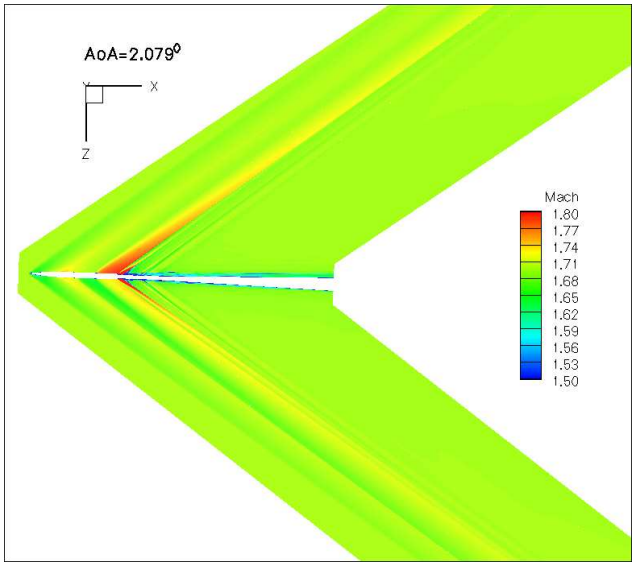

Figure 31: Mach contours at AoA=2.079

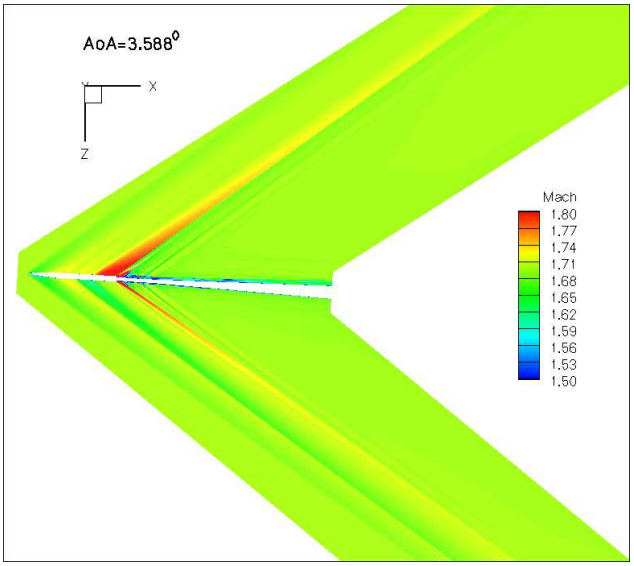

Figure 32: Mach contours at AoA=3.588

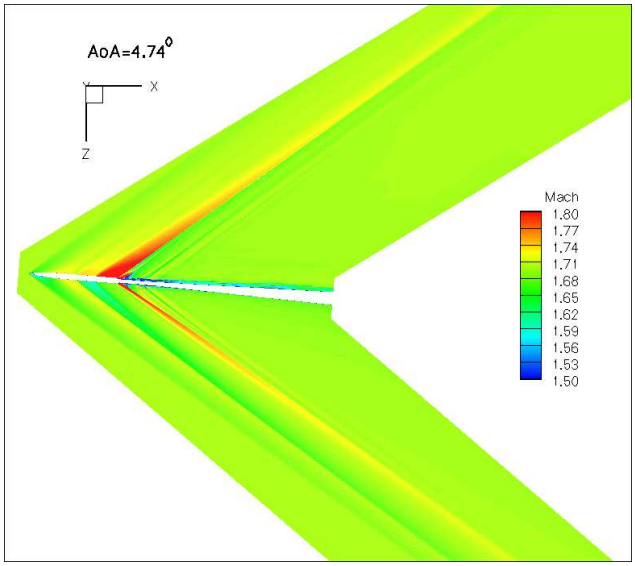

Figure 33: Mach contours at AoA=4.74

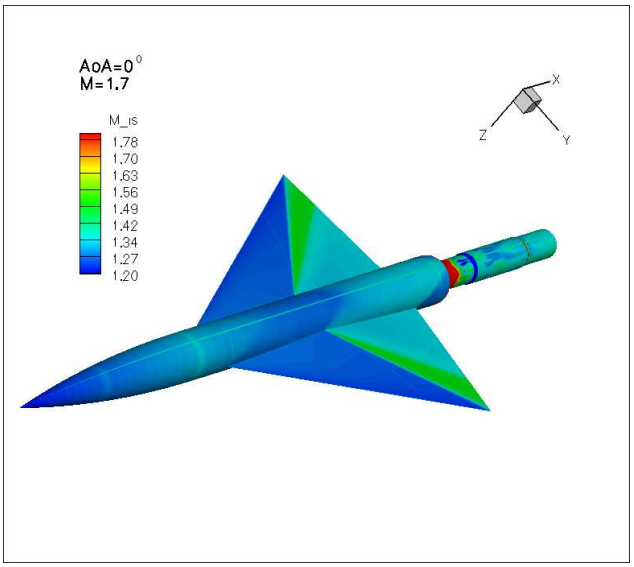

Figure 34: Isentropic mach number distribution around the body surface at AoA=0

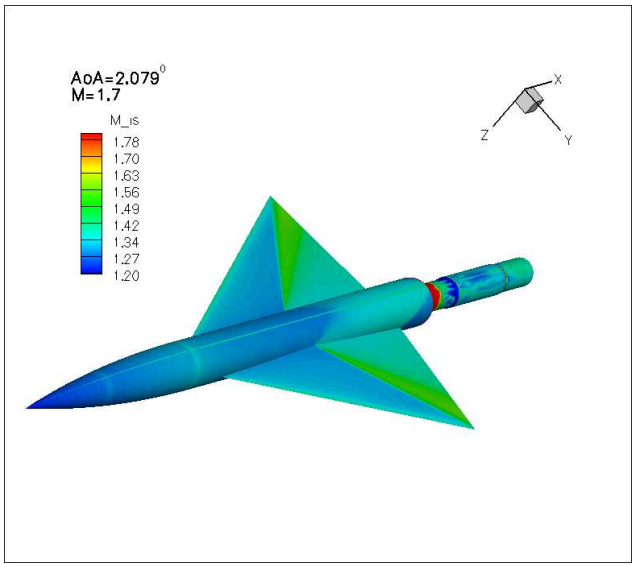

Figure 35: Isentropic mach number distribution around the body surface at AoA=2.079

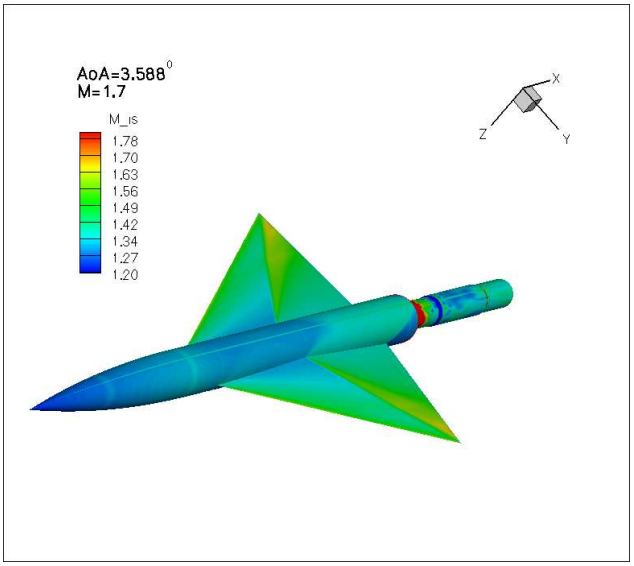

Figure 36: Isentropic mach number distribution around the body surface at AoA=3.588

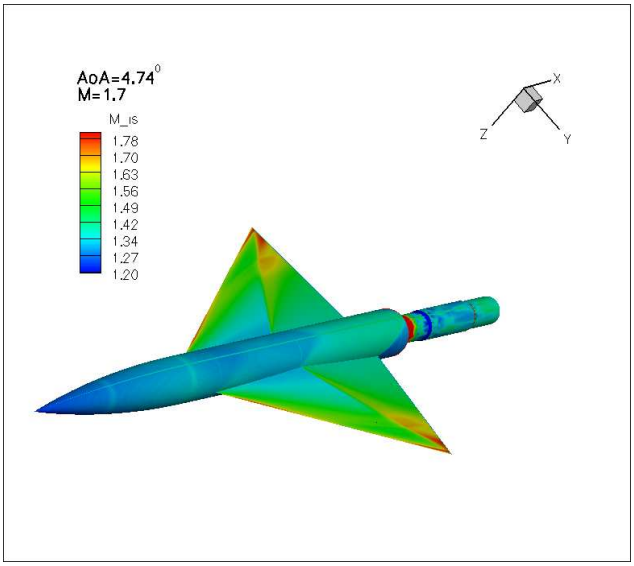

Figure 37: Isentropic mach number distribution around the body surface at AoA=4.74

References

[1] Durston, D. A. , " Sonic Boom Extrapolation and Sound Level Prediction." Unpublished Document, NASA Ames Research Center, Sept. 2009.

[2] Rallabhandi, S. K., "Advanced Sonic Boom Prediction Using Augmented Burgers Equation." 49th AIAA Aerospace Sciences Meeting including the New Horizons Forum and Aerospace Exposition, Orlando, Florida, Jan. 4-7, 2011.

[3] Rallabhandi, S. K., Li, Wu, Geiselhart, Kar, "Advanced Sonic Boom Prediction Using Augmented Burgers Equation." 48th AIAA Aerospace Sciences Meeting and Exhibit, Orlando FL, Jan. 4-7, 2010.

[4] Elmiligui, A., Cliff, S., Wilcox, F., Thomas, S.,, "Numerical Predictions of Sonic Boom Signatures for a Straight Line Segmented Leading Edge Model." Seventh International Conference on Computational Fluid Dynamics (ICCFD7) Big Island, Hawaii, July 9-13, 2012.

[5] Wintzer, M., Kroo, I., Aftosmis, M., and Nemec, M. , "Conceptual Design of Low Sonic Boom Aircraft Using Adjoint-Based CFD." Seventh International Conference on Computational Fluid Dynamics (ICCFD7) Big Island, Hawaii, July 9-13, 2012.

[6] Ishikawa, H., Tanaka, K., Makino, Y. and Yamamoto, K.,, "Sonic-Boom Prediction Using Euler CFD Codes With Structured/Unstructured Overset Method." 27th Congress of International Council of the Aeronautical Sciences, September 19-24, 2010.

[7] Park, M. A., Aftosmis, M. J., Campbell, R. L., Carter, M. B., Cliff, S. E., and Bangert, L. S.,, "Summary of the 2008 NASA Fundamental Aeronautics Program Sonic Boom Prediction Workshop." AIAA Paper 20130649, Jan, 2013.

[8] Aftosmis, M. J., and Nemec, M.,, "Cart3D Simulations for the First AIAA Sonic BoomPrediction Workshop." 52nd Aerospace Sciences Meeting, National Harbor, Maryland, January 13-17, 2014, 2014.

[9] Carlson, H. W. and Mack, R.J. and Morris, O. A. , " A Wind Tunnel Investigation of the Effect of Body Shape on Sonic Boom Pressure Distribution." NASA TN-D-3106, Nov. 1965.

[10] Zha, G.-C., Im, H. and Espinal, D., " Supersonic Bi-Directional Flying Wing, Part I: A novel concept for supersonic flight with high efficiency and low sonic boom ." AIAA Paper 2010-1013, 48th AIAA Aerospace Sciences Meeting, Orlando, FL, Jan. 4-6, 2010.

[11] Berger, C. and Carmona, K. and Im, H.-S. and Espinal, D.and Zha, G.-C., " Supersonic Bi-Directional Flying Wing Configuration with Low Sonic Boom and High Aerodynamic Efficiency." AIAA Paper 2011-3663, 29th AIAA Applied Aerodynamics Conference, Honolulu, Hawaii, 27-30 June 2011.

[12] Shen, Y.-Q. and Zha, G.-C. and Wang, B.-Y., " Improvement of Stability and Accuracy of Implicit WENO Scheme," *AIAA Journal*, vol. 47, No. 2, pp. 331–344, 2009.

[13] Shen, Y.-Q. and Zha, G.-C. , " Improvement of the WENO Scheme Smoothness Estimator," *International Journal for Numerical Methods in Fluids*, vol. DOI:10.1002/fld.2186, 2009.

[14] Shen, Y.-Q. and Zha, G.-C., " A Seventh-Order WENO Scheme and Its Applications." Submitted to SIAM Journal on Scientific Computing, Oct. 2010.

[15] B. Van Leer, "Towards the Ultimate Conservative Difference Scheme, III," *Journal of Computational Physics*, vol. 23, pp. 263–75, 1977.

[16] Y.-Q. Shen and G.-Z. Zha , "Generalized finite compact difference scheme for shock/complex flowfield interaction," *Journal of Computational Physics*, vol. doi:10.1016/j.jcp.2011.01.039, 2011.

[17] Shen, Y.-Q. and Zha, G.-C. and Chen, X.-Y., " High Order Conservative Differencing for Viscous Terms and the Application to Vortex-Induced Vibration Flows," *Journal of Computational Physics*, vol. 228(2), pp. 8283–8300, 2009.

[18] Y.-Q. Shen and G.-C. Zha, "Large Eddy Simulation Using a New Set of Sixth Order Schemes for Compressible Viscous Terms ," *Journal of Computational Physics*, vol. 229, pp. 8296–8312, 2010.

[19] Im, H-S., Chen, X-Y and Zha, G-C., " Detached Eddy Simulation of Rotating Stall Inception for a Full Annulus Transonic Rotor ," *AIAA Journal of Propulsion and Power*, vol. 28, No. 4, pp. 782–798, 2012.

[20] Im, H-S., Chen, X-Y., and Zha, G-C., "Prediction of a Supersonic Wing Flutter Boundary Using a High Fidelity Detached Eddy Simulation." AIAA Paper 2012-0039, 50th AIAA Aerospace Sciences Meeting, Tennessee,TN, submitted to AIAA Journal, 9-12 January 2012.

[21] Wang, B. Y and Zha, G.-C., "Detached-Eddy Simulation of Transonic Limit Cycle Oscillations Using High Order Schemes," *Journal of Computer & Fluids*, vol. 52, pp. 58–68, 2011.

[22] Wang, B. Y and Zha, G.-C., "Detached-Eddy Simulation of a Co-Flow Jet Airfoil at High Angle of Attack," *AIAA Journal of Aircraft*, vol. 48, 5, pp. 1495–1502, 2011.

[23] Im, H. and Zha, G., "Delayed Detached Eddy Simulation of the Aerodynamic Stall Flows Over the NACA0012 Airfoil." AIAA Paper 2011-1297, 49th AIAA Aerospace Sciences Meeting including, Orlando, Florida, 4 - 7 Jan 2011.

[24] Im, H-S. Chen, X.-Y. and Zha, G-C., "Simulation of 3D Multistage Axial Compressor Using a Fully Conservative Sliding Boundary Condition." ASME-IMECE 2011-62049, Proceedings of the ASME 2011 International Mechanical Engineering Congress & Exposition IMECE2011, Denver, Colorado, USA, Nov. 11-17, 2011.

[25] Im, H-S., Chen, X-Y and Zha, G-C., " Detached Eddy Simulation of Transonic Rotor Flutter Using a Fully Coupled Fluid-Structural Interaction ." ASME Paper GT2011-45437, ASME TURBO EXPO 2011, June 6-10, Vancouver, Canada, June 6-10, 2011.

[26] Im, H-S. and Zha, G-C., "Investigation of Co-Flow Jet Airfoil Mixing Mechanism Using Large Eddy Simulation." AIAA Paper 2011-3098, submitted to ASME J. of Fluid Engineering, (41st AIAA Fluid Dynamics Conference and Exhibit, 27-30 June 2011, Honolulu, Hawaii),, 2011.

[27] Wang, B. Y and Zha, G.-C., "High Fidelity Simulation of Nonlinear Fluid-Structural Interaction with Transonic Airfoil Limit Cycle Oscillations," *Journal of Fluids and Structures*, vol. doi:10.1016/j.jfluidstructs.2010.02.003, 2010.

[28] Wang, B.-Y. and Haddoukessouni, B. and Levy, J. and Zha, G.-C., "Numerical Investigations of Injection Slot Size Effect on the Performance of Co-Flow Jet Airfoil ," *AIAA Journal of Aircraft*, vol. 45, pp. 2084–2091, 2008.

[29] X.-Y. Chen, G.-C. Zha, and M.-T. Yang, "Numerical Simulation of 3-D Wing Flutter with Fully Coupled Fluid-Structural Interaction," *Journal of Computers & Fluids*, vol. 36, No. 5, pp. 856–867, 2007.

[30] X.-Y. Chen and G.-C. Zha, "Fully Coupled Fluid-Structural Interactions Using an Efficient High Resolution Upwind Scheme," *Journal of Fluids and Structures*, vol. 20, pp. 1105–1125, 2005.

[31] Z.-J. Hu and G.-C. Zha, "Calculations of 3D Compressible Using an Efficient Low Diffusion Upwind Scheme," *International Journal for Numerical Methods in Fluids*, vol. 47, pp. 253–269, 2004.

[32] Im, H-S. and Zha, G-C., "Effects of Rotor Tip Clearance on Tip Clearance Flow Potentially Leading to NSV in an Axial Compressor." ASME Paper GT2012-68148, IGTI Turbo Expo 2012, Copenhagen, Denmark, June 11-15, 2012.

[33] Im, H-S. and Zha, G-C., "Simulation of Non-synchronous Blade Vibration of an Axial Compressor Using a Fully Coupled Fluid-Structural Interaction." ASME Paper GT2012-68150, IGTI Turbo Expo 2012, Copenhagen, Denmark, June 11-15, 2012.

[34] Chen, X-Y., Im, H-S., and Zha, G-C., "Fully Coupled Fluid-Structural Interaction of a Transonic Rotor at Near-Stall Conditions Using Detached Eddy Simulation." AIAA Paper 2011-0228, 49th AIAA Aerospace Sciences Meeting including the New Horizons Forum and Aerospace Exposition 4 - 7 January 2011, Orlando, Florida, submitted to AIAA Journal, 2011.

[35] B.-Y. Wang and G.-C. Zha, "A General Sub-Domain Boundary Mapping Procedure For Structured Grid CFD Parallel Computation," *AIAA Journal of Aerospace Computing, Information, and Communication*, vol. 5, No.11, pp. 2084–2091, 2008.

[36] P. Roe, "Approximate Riemann Solvers, Parameter Vectors, and Difference Schemes," *Journal of Computational Physics*, vol. 43, pp. 357–372, 1981.

[37] G.-C. Zha, Y. Shen, and B. Wang, "An improved low diffusion E-CUSP upwind scheme ," *Journal of Computer & Fluids*, vol. 48, pp. 214–220, 2011.

[38] Wintzer, M. and Nemec, M. and Aftosmis, M. J., " Adjoint-Based Adaptive Mesh Refinement for Sonic Boom Prediction." AIAA 2008-6593, 26th AIAA Applied Aerodynamics Conference, Honolulu, Hawaii, 18-21 Aug. 2008.

[39] Thomas, C. L., " Extrapolation of Sonic Boom Pressure Signatures by the Waveform Parameter Method." NASA TN D-6832, June 1972.

[40] Casper, J. H. and Cliff, S. E. and Thomas, S. D. and Park, M. A. and McMullen, M.S. and Melton, J. E. and Durston, D. A., " Assessment of Near-Field Sonic Boom Simulation Tools." AIAA Paper 2008-6592, 26th AIAA Applied Aerodynamics Conference, Honolulu, Hawaii, 18-21 Aug. 2008.

[41] Ishikawa, H. and Makino, Y. and Ito, T. and Kuroda, F., " Sonic Boom Prediction Using Multi-Block Structured Grids CFD Code Considering Jet-On Effects." AIAA 2009-3508, June 2009.

[42] Choi, S. and Alonso, J. J. and Kroo, I. M. and Wintzer, M. , " Multi-Fidelity Design Optimization of Low Boom Supersonic Business Jets." AIAA 2004-4371, Aug. 30-Sept. 1, 2004.

[43] Hunton, L. W. and Mendoza, J. P. and Hicks, R. M., " Some Effects of Wing Planform on Sonic Boom." NASA TN D-7160, Jan 1973.